

APCodec: A Neural Audio Codec with Parallel Amplitude and Phase Spectrum Encoding and Decoding

Yang Ai, *Member, IEEE*, Xiao-Hang Jiang, Ye-Xin Lu, Hui-Peng Du, Zhen-Hua Ling, *Senior Member, IEEE*

Abstract—This paper introduces a novel neural audio codec targeting high waveform sampling rates and low bitrates named APCodec, which seamlessly integrates the strengths of parametric codecs and waveform codecs. The APCodec revolutionizes the process of audio encoding and decoding by concurrently handling the amplitude and phase spectra as audio parametric characteristics like parametric codecs. It is composed of an encoder and a decoder with the modified ConvNeXt v2 network as the backbone, connected by a quantizer based on the residual vector quantization (RVQ) mechanism. The encoder compresses the audio amplitude and phase spectra in parallel, amalgamating them into a continuous latent code at a reduced temporal resolution. This code is subsequently quantized by the quantizer. Ultimately, the decoder reconstructs the audio amplitude and phase spectra in parallel, and the decoded waveform is obtained by inverse short-time Fourier transform. To ensure the fidelity of decoded audio like waveform codecs, spectral-level loss, quantization loss, and generative adversarial network (GAN) based loss are collectively employed for training the APCodec. To support low-latency streamable inference, we employ feed-forward layers and causal convolutional layers in APCodec, incorporating a knowledge distillation training strategy to enhance the quality of decoded audio. Experimental results confirm that our proposed APCodec can encode 48 kHz audio at bitrate of just 6 kbps, with no significant degradation in the quality of the decoded audio. At the same bitrate, our proposed APCodec also demonstrates superior decoded audio quality and faster generation speed compared to well-known codecs, such as SoundStream, Encocdec, HiFi-Codec and AudioDec.

Index Terms—neural audio codec, amplitude spectrum, phase spectrum, neural network, knowledge distillation

I. INTRODUCTION

AUDIO codec, an important signal processing technique, compresses audio signals into discrete codes and then uses these codes to reconstruct the original audio. In general, an encoder, a quantizer, and a decoder are the three main components of an audio codec. The purpose of an audio codec is to utilize as few bits as possible (i.e., low bitrate) to store or transmit an audio signal while ensuring that the decoded audio quality doesn't undergo significant degradation.

This work was funded by the National Nature Science Foundation of China under Grant 62301521, the Anhui Provincial Natural Science Foundation under Grant 2308085QF200, and the Fundamental Research Funds for the Central Universities under Grant WK2100000033.

Y. Ai, X.-H. Jiang, Y.-X. Lu, H.-P. Du and Z.-H. Ling are with the National Engineering Research Center of Speech and Language Information Processing, University of Science and Technology of China, Hefei, 230027, China (e-mail: yangai@ustc.edu.cn, jiang_xiaohang@mail.ustc.edu.cn, yxlu0102@mail.ustc.edu.cn, redmist@mail.ustc.edu.cn, zhling@ustc.edu.cn).

Corresponding author: Zhen-Hua Ling.

Audio codec technology holds a central position in fields such as audio communication and transmission [1]–[4]. Recently, audio codec technology has also been gradually applied to some downstream tasks. For example, some researchers use the discrete codes generated by audio codecs as intermediate representations, combined with large language model technology, to achieve impressive zero-shot text-to-speech (TTS) results [5]–[9].

Audio codec has several key properties, which are also important metrics for evaluating the audio codec: 1) Decoded audio quality, reflecting the ability of an audio codec to restore compressed audio with as minimal loss as possible. 2) Bitrate, representing compression efficiency, indicating how many bits are used to represent the discrete codes generated by the audio codec. 3) Generation speed, denoting the overall running efficiency of audio encoding, quantization, and decoding. 4) Latency, a strict requirement for real-time audio communication, indicating the minimum amount of time needed for the codec to initiate its operations. In general, an audio codec that offers high decoded audio quality, low bitrate, fast generation speed and low latency is essential for applications such as audio communication. However, certain applications in downstream tasks typically prioritize the decoded audio quality over latency considerations. Factoring in latency can often have an impact on the overall results.

Audio codecs are generally categorized into two main types: parametric codecs and waveform codecs. The parametric codecs treat the characteristic parameters of audio signals as the objects for encoding and decoding, such as linear predictive coding (LPC) [10], Opus [11] and EVS [12]. Due to the short-term stationary nature of audio signals, the characteristic parameters are frame-level and have a low update frequency. Hence, the advantage of parametric codecs lies in their low bitrate. However, the drawback of such codecs is their poor decoded audio quality and susceptibility to noise. With the advancement of deep learning, researchers have employed neural vocoders to transform encoded characteristic parameters into audio waveforms, aiming to enhance the quality of decoded audio [13]–[17]. Recently, some approaches encode and decode the modified discrete cosine transform (MDCT) spectrum using neural networks, ultimately restoring the audio waveform through the inverse MDCT process [18], [19]. Unfortunately, as reported in [18], [19], these MDCT-based approaches typically necessitate high bitrate (>20 kbps at sampling rate of 48 kHz), thereby conflicting with the benefits of parametric codecs.

The waveform codecs aim at encoding the input audio waveform directly and reproducing a faithful reconstruction of the input audio waveform, such as pulse code modulation (PCM) [20]. Although waveform codecs can decode high-quality audio, they also require a higher bitrate, which increases storage and transmission costs. In recent times, end-to-end neural waveform codecs with raw waveform I/O have surfaced, offering a partial equilibrium between decoded audio quality and bitrate [21]–[26]. For example, SoundStream [25] and Encodec [26] employed the residual vector quantization (RVQ) mechanism [27] to reduce the bitrate, while utilizing the losses from the HiFi-GAN vocoder [28] to ensure the fidelity of the decoded audio. Recently, researchers have made improvements addressing the issues present in current end-to-end audio codecs, primarily focusing on quantization strategies. On the one hand, in applications such as audio communication, audio codecs have incorporated variations of RVQ to decrease bitrates and improve communication efficiency [29]–[31]. On the other hand, in downstream tasks such as TTS, efforts have been undertaken to introduce or disentangle semantic information during the quantization stage, aiming to tailor the approach to the specific tasks [7]–[9]. Moreover, there have been endeavors to improve the model structure [30] or incorporate additional signal processing techniques in codecs [32]. Although these codecs have indeed enhanced the decoded audio quality and decreased bitrates, they still required more than a hundred times the downsampling and upsampling operations due to the direct waveform encoding and decoding, leading to high model complexity. Besides, direct waveform encoding and decoding could also potentially result in low generation efficiency. Some recent works have also overlooked considerations for low latency, making it challenging to achieve streamable inference [29], [30].

Beyond the aforementioned challenges, encompassing bitrate, generation speed, and latency in existing audio codecs, there is presently scant research devoted to audio codecs tailored for higher waveform sampling rates (e.g., 48 kHz). Currently, neural audio codecs (e.g., SoundStream and HiFi-Codec) are mostly designed for processing audio at sampling rates of 16 kHz or 24 kHz. This limitation hinders the utilization of audio codecs for compressing high-sampling-rate audio data and poses challenges for downstream tasks like TTS, which aim to meet the demand for higher quality speech generation. The aforementioned MDCT-based parametric codecs [18], [19], while targeted at 48 kHz audio, demands an excessively high bitrate. Although AudioDec [33] can achieve 48 kHz audio codec at bitrate of 12.8 kbps, it still requires the integration of a neural vocoder and the adoption of a multi-stage training strategy, as reported in [33].

To address the aforementioned challenges, this paper proposes a novel neural audio codec named APCodec. It endeavors to provide high-quality decoded audio, while maintaining a low bitrate, fast generation speed, and low latency, specifically tailored for 48 kHz audio. Like parametric codecs, the proposed APCodec regards amplitude and phase spectra as audio parameter characteristics during the encoding and decoding processes, rather than directly processing the raw waveform.

A notable advantage of this approach lies in its simplicity, as it only requires uncomplicated downsampling to obtain latent codes at an appropriately low sampling rate, thereby effectively reducing the bitrate. RVQ [27] is also utilized for code quantization to further reduce the bitrate. With the objective of achieving faithful waveform reconstruction akin to waveform codecs, a comprehensive combination of spectral-level loss, quantization loss and generative adversarial network (GAN) based loss are employed to train the APCodec. To attain streamable inference, a low-latency implementation is achieved by integrating feed-forward layers and causal convolutional layers, complemented by the application of a knowledge distillation training strategy. The resulting fixed latency is only 6.67 ms for the 48 kHz audio codec. Experimental results have confirmed that the proposed APCodec can achieve high-quality 48 kHz audio codec at a bitrate of only 6 kbps with only $8\times$ downsampling/upsampling. At the same bitrate, our proposed APCodec significantly outperforms several well-known neural codecs, e.g., SoundStream [25], Encodec [26], HiFi-Codec [29] and AudioDec [33] in terms of decoded audio quality. The APCodec also demonstrates the fastest generation speed, attaining an impressive $89\times$ real-time performance on GPU and $5.8\times$ real-time performance on CPU. This remarkable acceleration is attributed to its comprehensive all-frame-level processing.

There are three main contributions of the proposed APCodec. Firstly, the APCodec targets audio encoding and decoding at high sampling rates and low bitrates, meeting the demands for high-sampling-rate audio compression and generation. Secondly, the APCodec utilizes amplitude and phase spectra as the encoding and decoding entities, rather than waveforms, thereby further enhancing generation efficiency. Thirdly, the APCodec introduces knowledge distillation to enhance the effectiveness of causal audio codec models. This approach provides valuable insights into realizing low-latency implementations in contemporary audio codec technology.

This paper is organized as follows: In Section II, we briefly review the advanced neural audio codecs. In Section III, we provide details on our proposed APCodec. In Section IV, we present our experimental results. Finally, we give conclusions in Section V.

II. RELATED WORKS

The focus of this paper is the neural audio codec. SoundStream [25] and Encodec [26] are earlier well-known neural audio codec baseline models that directly encode and decode audio waveforms. They consist of an encoder, a quantizer, and a decoder. The encoder and decoder are designed based on causal convolutional layers for low-latency streamable inference, while the quantizer employs RVQ to reduce the bitrate. GAN-based loss, inspired by HiFi-GAN [28], along with reconstruction loss, quantization loss, and other components, is utilized to train the encoder, quantizer, and decoder jointly.

Recently, researchers have proposed several improvement methods around the framework of SoundStream and Encodec. Regarding quantization strategy, HiFi-Codec [29] has introduced group RVQ (GRVQ) to reduce information redundancy

in RVQ. This allows for high-quality audio codec with less codebooks, resulting in a reduced bitrate. CBRC [30] proposes group-wise and beam-search RVQ (GB-RVQ) to mitigate quantization errors, thereby enhancing the decoded audio quality. Several latest speech codecs such as SpeechTokenizer [7], RepCodec [8] and TiCodec [9], also attempt to introduce or disentangle semantic information within the quantized discrete codes, making them better suited for downstream tasks such as TTS. In terms of model architecture, CBRC [30] introduces convolutional and bidirectional recurrent neural network (CBRN) blocks to replace conventional convolutional layers, aiming to enhance the quality of decoded audio. Additionally, some efforts leverage other tools to achieve improvements in neural audio codecs [17], [32]. For example, CQNV [17] initially encodes and quantizes 8 kHz speech, and finally restores 16 kHz speech directly through a HiFi-GAN vocoder, implying a process of bandwidth extension (BWE). This method of encoding low-sampling-rate speech contributes to reducing the bitrate.

The aforementioned neural audio codecs (e.g., SoundStream and HiFi-Codec) are designed to handle 16 kHz or 24 kHz audio. For high-sampling-rate audio codecs, there have been efforts to perform encoding, quantization, and decoding in the MDCT domain [18], [19]. However, the required bitrate is very high, thus limiting the compression efficiency. At present, there is still a noticeable deficiency in the field of audio codec within other spectral domains (e.g., amplitude and phase spectra). The recently proposed AudioDec [33] has been reported to achieve a 48 kHz audio codec at 12.8 kbps. However, AudioDec employs a sophisticated two-stage training mode, and experimental findings reveal that achieving high-quality audio decoding still necessitates the support of the HiFi-GAN vocoder.

III. PROPOSED METHODS

Unlike some well-known neural waveform codecs (e.g., SoundStream [25] and Encodec [26]), our proposed APCodec encodes and quantizes amplitude and phase spectra extracted from the audio waveform through short-time Fourier transform (STFT). Finally, it decodes the quantized codes into amplitude and phase spectra and restores the audio waveform through inverse STFT (ISTFT). Subsequently, we will present a detailed overview of the model structure and training criteria of the proposed APCodec. Additionally, we will discuss the low-latency implementation for APCodec.

A. Model Structure

As illustrated in Fig. 1, the proposed APCodec consists of an encoder, a quantizer and a decoder. The APCodec utilizes amplitude and phase spectra as audio parametric characteristics for encoding and decoding, incorporating the advantages of parametric codecs to reduce bitrates. The specific structures of these three components are outlined as follows.

1) *Encoder*: As illustrated in Fig. 1, the encoder takes the log amplitude spectrum $\mathbf{A} \in \mathbb{R}^{F \times N}$ and phase spectrum $\mathbf{P} \in \mathbb{R}^{F \times N}$ extracted from the audio waveform $\mathbf{x} \in \mathbb{R}^T$ using STFT as inputs and encodes them into a continuous

latent code $\mathbf{C} \in \mathbb{R}^{F_c \times N_c}$ that contains fused amplitude and phase information in parallel. Here, T represents the number of time-domain waveform samples, and F and N respectively represent the number of spectral frames and frequency bins. Assuming the sampling rate of \mathbf{x} is f_s and the frame shift of the STFT is w_s , the resulting sampling rate for the extracted amplitude and phase spectra is f_s/w_s , and it holds that $T = F \cdot w_s$. F_c and N_c denote the number of frames and dimensionality of the code, respectively.

The encoder comprises parallel amplitude and phase sub-encoders that share an identical network architecture, as shown in Fig. 1. In the amplitude/phase sub-encoder, the input amplitude/phase spectrum is initially processed through an input 1D convolutional layer (channel size = C), a layer normalization [34] and then undergoes deep processing through a modified ConvNeXt v2 network. The output of the modified ConvNeXt v2 network is further processed by a layer normalization and a feed-forward layer with C nodes. The 1D downsampling convolutional layer (channel size = $C/2$ and stride = D) serves as the ultimate component in the amplitude/phase sub-encoder, further downsampling the output features of the feed-forward layer by a factor of D and reducing its dimensionality by half to generate amplitude/phase continuous latent code $\mathbf{C}_A/\mathbf{C}_P \in \mathbb{R}^{F_c \times (C/2)}$. Therefore, we have $F_c = F/D$.

The modified ConvNeXt v2 network, which is constructed by cascading 8 identical modified ConvNeXt v2 blocks, serves as the backbone of both encoder and decoder. The modified ConvNeXt v2 block has been adapted from the ConvNeXt v2 block originally designed for image processing [35]. The primary modification involves replacing 2D convolutions with 1D ones, thereby tailoring the block to better suit the processing of audio signals. As shown in Fig. 2, in each modified ConvNeXt v2 block, the input sequentially passes through a 1D depth-wise convolutional layer (channel size = C), a layer normalization, a feed-forward layer with C_H nodes that projects features into a higher dimensionality (i.e., $C_H > C$), a Gaussian error linear unit (GELU) activation [36], a global response normalization (GRN) layer [35], another feed-forward layer with C nodes that projects features back to the original dimensionality, and finally superimposes with the input (i.e., residual connections) to obtain the output.

To aggregate both the amplitude and phase information, we concatenate the amplitude code and phase code along the dimension axis to obtain a fused latent code $[\mathbf{C}_A, \mathbf{C}_P] \in \mathbb{R}^{F_c \times C}$. Then, a dimensionality-reduction 1D convolutional layer (channel size = N_c) is used to significantly reduce the dimension of this fused code, resulting in a low-dimensional fused continuous latent code $\mathbf{C} \in \mathbb{R}^{F_c \times N_c}$ which combines both the amplitude and phase information. The reason for reducing the dimensionality of the continuous latent code \mathbf{C} is to concurrently decrease the dimensionality of codebooks during subsequent quantization process, facilitating the storage and transmission of codebooks. The sampling rate of \mathbf{C} is $f_s/w_s/D$, which is one- D of the sampling rate of the amplitude and phase spectra.

Therefore, the functionality of the encoder can be expressed

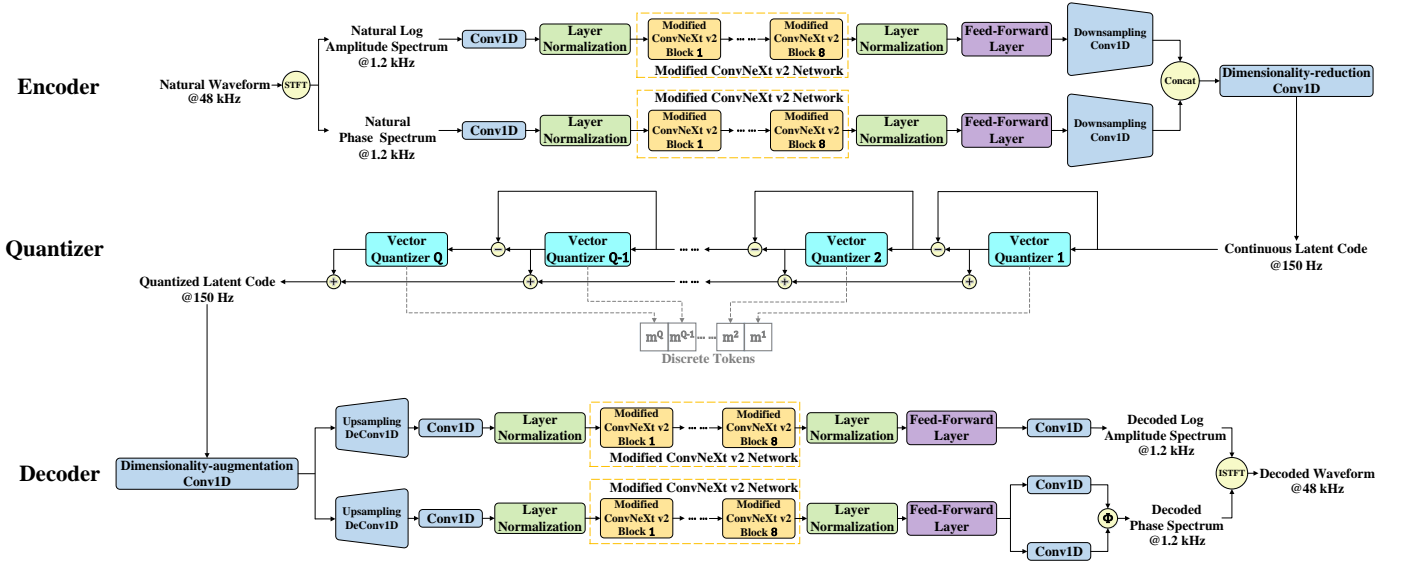


Fig. 1. Details of the model structure of the proposed APCodec. Here, *Conv1D*, *DeConv1D*, *Concat*, Φ , *STFT* and *ISTFT* represent the 1D convolutional layer, 1D deconvolutional layer, concatenation, phase calculation formula, short-time Fourier transform and inverse short-time Fourier transform, respectively.

by the following formula:

$$\mathbf{C} = \text{Encoder}(\mathbf{A}, \mathbf{P}). \quad (1)$$

2) *Quantizer*: As illustrated in Fig. 1, the quantizer discretizes the continuous latent code $\mathbf{C} \in \mathbb{R}^{F_c \times N_c}$ and generates the quantized latent code $\hat{\mathbf{C}} \in \mathbb{R}^{F_c \times N_c}$ based on trainable codebooks. RVQ strategy is utilized in the quantizer to lower the bitrate. The quantizer consists of Q vector quantizers (VQs), each of which has a trainable codebook $\mathbf{B}^q \in \mathbb{R}^{N_c \times M}$, $q = 1, \dots, Q$, where M represents the number of vectors. The quantization process is as follows. For the first VQ, the input is the continuous latent code \mathbf{C} and we let $\mathbf{L}^1 = \mathbf{C}$. Taking the i -th ($i = 1, 2, \dots, F_c$) frame of \mathbf{L}^1 , denoted as $\mathbf{l}_i^1 \in \mathbb{R}^{N_c}$, as an example, we first calculate the Euclidean distance between \mathbf{l}_i^1 and each vector in \mathbf{B}^1 , then choose the vector with the smallest distance as the quantized code $\hat{\mathbf{l}}_i^1 \in \mathbb{R}^{N_c}$, and save its index in \mathbf{B}^1 as $m_i^1 \in \{1, 2, \dots, M\}$. Therefore, for all frames, the quantized code and index can be represented as $\hat{\mathbf{L}}^1 = [\hat{\mathbf{l}}_1^1, \dots, \hat{\mathbf{l}}_i^1, \dots, \hat{\mathbf{l}}_{F_c}^1]^\top \in \mathbb{R}^{F_c \times N_c}$ and $\mathbf{m}^1 = [m_1^1, \dots, m_i^1, \dots, m_{F_c}^1]^\top \in \mathbb{R}^{F_c}$, respectively. Finally, the quantization residual $\mathbf{L}^2 = \mathbf{L}^1 - \hat{\mathbf{L}}^1$ is computed as the input for the next VQ. Repeat the above process sequentially until the final VQ's operation is completed. The quantizer eventually generates the quantized latent code as the sum of the outputs from each VQ, i.e., $\hat{\mathbf{C}} = \sum_{q=1}^Q \hat{\mathbf{L}}^q$. The VQ index vectors (i.e., discrete tokens) $\mathbf{m}^1, \mathbf{m}^2, \dots, \mathbf{m}^Q$ are represented in binary. Therefore, the bitrate measured in kbps of the APCodec can be calculated as follows:

$$\text{Bitrate} = \frac{1}{1000} \cdot \frac{f_s}{w_s \cdot D} \cdot Q \cdot \log_2 M. \quad (2)$$

The functionality of the quantizer can be expressed by the following formula:

$$\hat{\mathbf{C}}, \mathbf{m}^1, \mathbf{m}^2, \dots, \mathbf{m}^Q = \text{Quantizer}(\mathbf{C} | \mathbf{B}^1, \mathbf{B}^2, \dots, \mathbf{B}^Q). \quad (3)$$

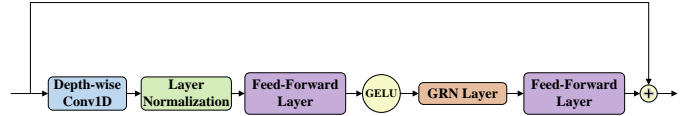


Fig. 2. Details of the modified ConvNeXt v2 block. Here, *Conv1D*, *GELU* and *GRN* represent the 1D convolutional layer, Gaussian error linear unit and global response normalization, respectively.

For applications such as audio communication, discrete tokens (binary form) $\mathbf{m}^1, \mathbf{m}^2, \dots, \mathbf{m}^Q$ are sent from the transmitter to the receiver. The receiver then transforms the discrete tokens into quantized codes based on the codebooks and proceeds with the subsequent decoding process. For downstream tasks such as TTS, discrete tokens are used as intermediate representations to bridge text and speech.

3) *Decoder*: As illustrated in Fig. 1, the decoder decodes the log amplitude spectrum $\hat{\mathbf{A}} \in \mathbb{R}^{F_c \times N}$ and phase spectrum $\hat{\mathbf{P}} \in \mathbb{R}^{F_c \times N}$ in parallel from the input quantized latent code $\hat{\mathbf{C}} \in \mathbb{R}^{F_c \times N_c}$, and finally reconstructs the decoded waveform $\hat{\mathbf{x}} \in \mathbb{R}^T$ through ISTFT. The structure of the decoder is roughly symmetrical to that of the encoder. The parallel amplitude and phase sub-decoders are the primary components of the decoder. The quantized latent code $\hat{\mathbf{C}}$ is first dimensionally restored through a 1D dimensionality-augmentation convolutional layer (channel size = $C/2$) to be used as input for both the amplitude and phase sub-decoders. In the amplitude sub-decoder, the input is first upsampled D times through a 1D deconvolutional layer (channel size = C and stride = D), a layer normalization and then processed by a modified ConvNeXt v2 network along with a layer normalization and a feed-forward layer with C nodes. Finally, a 1D output convolutional layer (channel size = N) is adopted to predict the decoded log amplitude spectrum $\hat{\mathbf{A}}$. The sole distinction between the phase sub-decoder and the amplitude sub-decoder lies in the utilization of a phase parallel estimation

architecture proposed in our previous publication [37] at the output end of the phase sub-decoder. The parallel estimation architecture ensures the direct prediction of wrapped phase spectra, consisting of two identical parallel 1D convolutional layers (channel size = N) and a phase calculation formula Φ . Assume the outputs of the two parallel layers are $\hat{\mathbf{R}} \in \mathbb{R}^{F \times N}$ and $\hat{\mathbf{I}} \in \mathbb{R}^{F \times N}$, respectively, then the phase spectrum is calculated by $\hat{\mathbf{P}} = \Phi(\hat{\mathbf{R}}, \hat{\mathbf{I}})$. Function Φ is calculated element-wise. For $\forall R \in \mathbb{R}$ and $I \in \mathbb{R}$, we have

$$\Phi(R, I) = \arctan\left(\frac{I}{R}\right) - \frac{\pi}{2} \cdot \text{Sgn}^*(I) \cdot [\text{Sgn}^*(R) - 1], \quad (4)$$

and $\Phi(0, 0) = 0$. When $x \geq 0$, $\text{Sgn}^*(x) = 1$; or, $\text{Sgn}^*(x) = -1$.

Therefore, the functionality of the decoder and the process of decoded waveform reconstruction can be expressed by the following formula:

$$\hat{\mathbf{A}}, \hat{\mathbf{P}} = \text{Decoder}(\hat{\mathbf{C}}), \quad (5)$$

$$\hat{\mathbf{S}} = \exp(\hat{\mathbf{A}}) \cdot \exp(j\hat{\mathbf{P}}), \quad (6)$$

$$\hat{\mathbf{x}} = \text{ISTFT}(\hat{\mathbf{S}}), \quad (7)$$

where $\hat{\mathbf{S}} \in \mathbb{C}^{F \times N}$ is the decoded short-time complex spectrum.

B. Training Criteria

A comprehensive combination of spectral-level loss, quantization loss and GAN-based loss are employed to jointly train the encoder, quantizer, and decoder in the APCodec. These loss functions ensure the faithful reproduction of decoded audio in a comprehensive manner, highlighting how APCodec has assimilated the advantages of waveform codecs. These losses are visualized in Fig. 3.

1) *Spectral-level Loss*: The spectral-level loss is defined on the amplitude spectrum, phase spectrum, short-time complex spectrum and mel spectrogram, respectively, inspired by our previous publications [37], [38].

The loss defined on the amplitude spectrum \mathcal{L}_A is the mean square error (MSE) between the decoded log amplitude spectrum $\hat{\mathbf{A}} \in \mathbb{R}^{F \times N}$ and the natural one $\mathbf{A} \in \mathbb{R}^{F \times N}$, i.e.,

$$\mathcal{L}_A = \frac{1}{FN} \cdot \mathbb{E}_{(\hat{\mathbf{A}}, \mathbf{A})} \left\| \hat{\mathbf{A}} - \mathbf{A} \right\|_F^2, \quad (8)$$

where $\|\cdot\|_F$ denotes the Frobenius norm.

The loss defined on the phase spectrum \mathcal{L}_P consists of anti-wrapping instantaneous phase (AW-IP) loss \mathcal{L}_{IP} , anti-wrapping group delay (AW-GD) loss \mathcal{L}_{GD} and anti-wrapping instantaneous angular frequency (AW-IAF) loss \mathcal{L}_{IAF} which are all defined between the decoded phase spectrum $\hat{\mathbf{P}} \in \mathbb{R}^{F \times N}$ and the natural one $\mathbf{P} \in \mathbb{R}^{F \times N}$. To avoid the training error expansion issue caused by phase wrapping, we activate phase errors using an anti-wrapping function $f_{AW}(x) = |x - 2\pi \cdot \text{round}(\frac{x}{2\pi})|$, $x \in \mathbb{R}$. The definitions of these three losses are as follows:

$$\mathcal{L}_{IP} = \frac{1}{FN} \cdot \mathbb{E}_{(\hat{\mathbf{P}}, \mathbf{P})} \left\| f_{AW}(\hat{\mathbf{P}} - \mathbf{P}) \right\|_1, \quad (9)$$

$$\mathcal{L}_{GD} = \frac{1}{FN} \cdot \mathbb{E}_{(\hat{\mathbf{P}}, \mathbf{P})} \left\| f_{AW}(\Delta_{DF}\hat{\mathbf{P}} - \Delta_{DF}\mathbf{P}) \right\|_1, \quad (10)$$

$$\mathcal{L}_{IAF} = \frac{1}{FN} \cdot \mathbb{E}_{(\hat{\mathbf{P}}, \mathbf{P})} \left\| f_{AW}(\Delta_{DT}\hat{\mathbf{P}} - \Delta_{DT}\mathbf{P}) \right\|_1, \quad (11)$$

where $\|\cdot\|_1$ denotes the L1 norm (entrywise form). Δ_{DF} and Δ_{DT} represent the differential along the frequency axis and time axis, respectively. \mathcal{L}_P is the sum of the AW-IP loss, AW-GD loss and AW-IAF loss, i.e.,

$$\mathcal{L}_P = \mathcal{L}_{IP} + \mathcal{L}_{GD} + \mathcal{L}_{IAF}. \quad (12)$$

Furthermore, we also establish the short-time complex spectrum loss, denoted as \mathcal{L}_S , to quantify the error in the decoded short-time complex spectrum $\hat{\mathbf{S}} \in \mathbb{C}^{F \times N}$ (i.e., Equation 6). This loss encompasses the real and imaginary part loss \mathcal{L}_{RI} , as well as a consistency loss \mathcal{L}_C . \mathcal{L}_{RI} is defined as the mean absolute error (MAE) between the real and imaginary parts of $\hat{\mathbf{S}}$ and the natural ones, i.e.,

$$\mathcal{L}_{RI} = \frac{1}{FN} \cdot \mathbb{E}_{(\hat{\mathbf{S}}, \mathbf{S})} \left(\left\| \text{Re}(\hat{\mathbf{S}}) - \text{Re}(\mathbf{S}) \right\|_1 + \left\| \text{Im}(\hat{\mathbf{S}}) - \text{Im}(\mathbf{S}) \right\|_1 \right), \quad (13)$$

where $\mathbf{S} \in \mathbb{C}^{F \times N}$ is the natural short-time complex spectrum extracted from \mathbf{x} . Re and Im are the real part calculation and imaginary part calculation, respectively. It reflects the differences between the decoded short-time complex spectrum and the natural one. To mitigate the inconsistency issues of STFT and narrow the consistency gap between $\hat{\mathbf{S}}$ and the consistent short-time complex spectrum $\tilde{\mathbf{S}} = \text{STFT}(\text{ISTFT}(\hat{\mathbf{x}}))$, we define the consistency loss as follows:

$$\mathcal{L}_C = \frac{1}{FN} \cdot \mathbb{E}_{(\hat{\mathbf{S}}, \tilde{\mathbf{S}})} \left(\left\| \text{Re}(\hat{\mathbf{S}}) - \text{Re}(\tilde{\mathbf{S}}) \right\|_F^2 + \left\| \text{Im}(\hat{\mathbf{S}}) - \text{Im}(\tilde{\mathbf{S}}) \right\|_F^2 \right). \quad (14)$$

\mathcal{L}_S is a linear combination of \mathcal{L}_{RI} and \mathcal{L}_C , i.e.,

$$\mathcal{L}_S = \lambda_{RI}\mathcal{L}_{RI} + \mathcal{L}_C, \quad (15)$$

where λ_{RI} is hyperparameter.

Ultimately, we articulate the loss on the mel spectrogram as a fusion of MAE and MSE between the extracted mel spectrogram $\hat{\mathbf{M}} \in \mathbb{R}^{F \times M}$ and $\mathbf{M} \in \mathbb{R}^{F \times M}$ derived from decoded waveform $\hat{\mathbf{x}}$ and natural one \mathbf{x} , respectively, i.e.,

$$\mathcal{L}_M = \frac{1}{FM} \cdot \mathbb{E}_{(\hat{\mathbf{M}}, \mathbf{M})} \left(\left\| \hat{\mathbf{M}} - \mathbf{M} \right\|_1 + \left\| \hat{\mathbf{M}} - \mathbf{M} \right\|_F^2 \right), \quad (16)$$

where M is the dimensionality of the mel spectrogram.

Overall, the spectral-level loss is a linear combination of \mathcal{L}_A , \mathcal{L}_P , \mathcal{L}_S and \mathcal{L}_M , i.e.,

$$\mathcal{L}_{spec} = \mathcal{L}_A + \lambda_P\mathcal{L}_P + \lambda_S\mathcal{L}_S + \lambda_M\mathcal{L}_M, \quad (17)$$

where λ_P , λ_S and λ_M are hyperparameters.

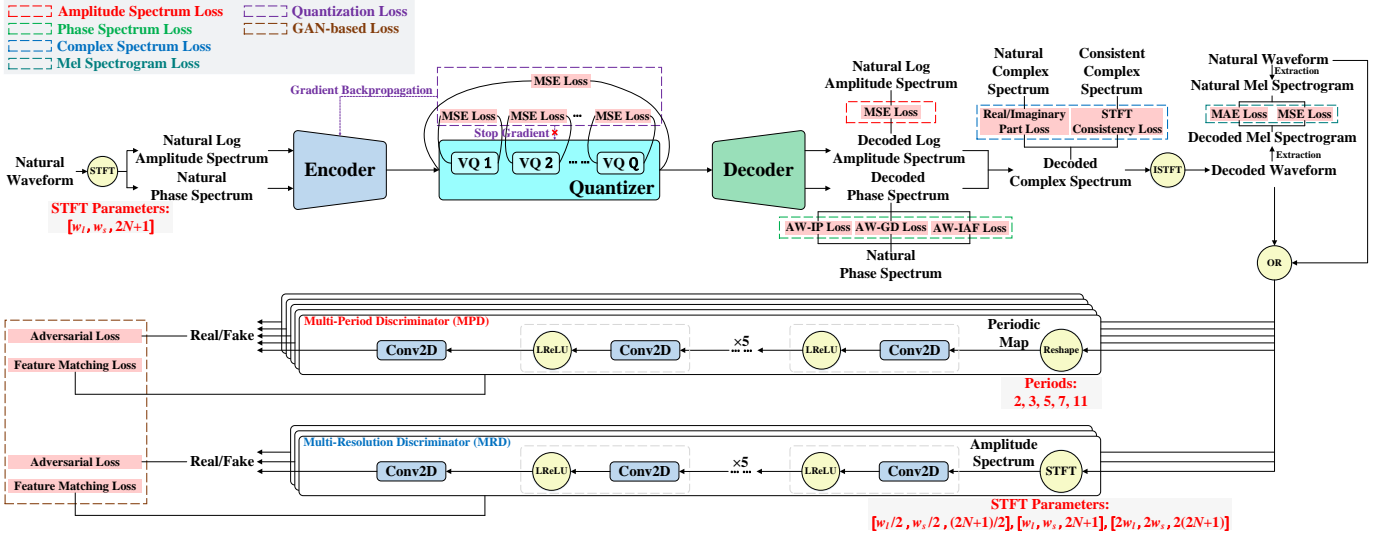


Fig. 3. Details of the training losses of the proposed APCodec. Here, VQ , $Conv2D$ and $LReLU$ represent the vector quantizer, 2D convolutional layer and leaky rectified linear unit, respectively. Other abbreviations are the same as those used in Fig. 1. The structure of the encoder, quantizer, and decoder is simplified.

2) *Quantization Loss*: The quantization loss \mathcal{L}_Q aims to reduce quantization errors, defined as the MSE between the input and output of the quantizer, as well as the MSE between the input and output of each VQ within the quantizer, i.e.,

$$\mathcal{L}_Q = \frac{1}{F_c N_c} \cdot \mathbb{E}_{(\hat{c}, c)} \|\hat{c} - c\|_F^2 + \frac{1}{Q F_c N_c} \cdot \sum_{q=1}^Q \mathbb{E}_{(\hat{c}_q, \hat{c}_{q-1})} \|\hat{c}_q - \hat{c}_{q-1}\|_F^2, \quad (18)$$

where $\hat{c}_q \in \mathbb{R}^{F_c \times N_c}$ ($1 \leq q \leq Q$) is the output of the q -th VQ and $\hat{c}_0 = c$. As shown in Fig. 3, the quantization loss \mathcal{L}_Q is used exclusively to update the encoder through gradient backpropagation while bypassing the quantizer.

3) *GAN-based Loss*: For GAN-based loss, the APCodec incorporates a multi-period discriminator (MPD) [28] to capture audio periodic patterns and a multi-resolution discriminator (MRD) [39] to ensure the high quality of the audio spectrum across various time and frequency scales. As shown in Fig. 3, the MPD comprises 5 parallel sub-MPDs. Each sub-MPD reshapes the input decoded waveform \hat{x} or natural waveform x into a 2D periodic map according to the set period. This periodic map is subsequently processed through 5 sequential blocks, each of which consists of a 2D convolutional layer and a leaky rectified linear unit (LReLU) activation [40]. Finally, the output undergoes further processing through a 2D output convolutional layer to produce a discriminative score. The periods are respectively set to 2, 3, 5, 7, and 11.

As shown in Fig. 3, the MRD comprises 3 parallel sub-MRDs. Each sub-MRD extracts the amplitude spectrum from \hat{x} or x according to specified STFT parameters. Subsequently, the amplitude spectrum undergoes processing through a network identical to that of the sub-MRD (with different convolutional layer parameters), resulting in the output of a discriminative score. Assuming the STFT parameters for extracting the input amplitude and phase spectra for the encoder are: [frame length, frame shift, FFT point number] = $[w_l, w_s, 2N + 1]$. We set the STFT parameters for the three

sub-MRDs as $[w_l/2, w_s/2, (2N + 1)/2]$, $[w_l, w_s, 2N + 1]$ and $[2w_l, 2w_s, 2(2N + 1)]$, respectively.

The adversarial loss in the form of hinge GAN is utilized. For a certain sub-discriminator D^* in MPD and MRD, the adversarial losses for generator and discriminator are as follows:

$$\mathcal{L}_{adv-G}^* = \mathbb{E}_{\hat{x}} \max(0, 1 - D^*(\hat{x})), \quad (19)$$

$$\mathcal{L}_{adv-D}^* = \mathbb{E}_{(\hat{x}, x)} [\max(0, 1 - D^*(x)) + \max(0, 1 + D^*(\hat{x}))]. \quad (20)$$

Additionally, feature matching loss \mathcal{L}_{FM}^* [41] is utilized, characterized by the summation of the MAE between the corresponding intermediate layer outputs of sub-discriminator D^* when provided with inputs \hat{x} or x .

Therefore, the GAN-based losses for generator and discriminator are respectively defined by the following expressions:

$$\mathcal{L}_G = \sum_{i=1}^5 (\mathcal{L}_{adv-G}^{P_i} + \mathcal{L}_{FM}^{P_i}) + \lambda_{MRD} \sum_{j=1}^3 (\mathcal{L}_{adv-G}^{R_j} + \mathcal{L}_{FM}^{R_j}), \quad (21)$$

$$\mathcal{L}_D = \sum_{i=1}^5 \mathcal{L}_{adv-D}^{P_i} + \lambda_{MRD} \sum_{j=1}^3 \mathcal{L}_{adv-D}^{R_j}, \quad (22)$$

where the superscripts P_i and R_j represent i -th sub-MPD and j -th sub-MRD, respectively. λ_{MRD} is hyperparameter.

4) *Training Process*: The final generator loss is a linear combination of the aforementioned spectral-level loss, quantization loss and GAN-based loss, i.e.,

$$\mathcal{L} = \lambda_{spec} \mathcal{L}_{spec} + \lambda_Q \mathcal{L}_Q + \mathcal{L}_G, \quad (23)$$

where λ_{spec} and λ_Q are hyperparameters. The training of the APCodec follows the standard training process of GAN, i.e., using \mathcal{L} and \mathcal{L}_D to train the generator (i.e., the encoder, quantizer and decoder) and discriminators (i.e., the MPD and MRD) alternately.

C. Low-latency Implementation by Knowledge Distillation

To attain low-latency streamable inference, we implement modifications to specific components of the APCodec, covering the following three aspects. 1) Unlike some well-known codecs like SoundStream [25] and Encodec [26] that employ causal convolutions, the streamable APCodec replaces all non-causal convolutional layers (excluding up-sampling/downsampling layers) with feed-forward layers. This approach is conducive to reducing model size and improving generation efficiency; 2) Replacing the original non-causal upsampling deconvolutional layers with causal ones; 3) Setting the kernel size of the downsampling convolutional layer to be smaller than the downsampling rate D .

However, with the aforementioned modifications, the streamable APCodec, compared to the original non-streamable APCodec, inevitably leads to a deterioration in decoded audio quality. Therefore, we introduce a knowledge distillation training strategy, utilizing a well-trained non-streamable APCodec as the teacher model to guide the training of the streamable APCodec (i.e., the student model). To establish a connection between the teacher model and the student model, we introduce a knowledge distillation loss \mathcal{L}_{KD} , defined as the MSE between the features of the two models at corresponding positions. These positions encompass the output of all convolutional layers, feed-forward layers, modified ConvNeXt v2 blocks, and the quantizer in Fig. 1. At the training stage, the streamable APCodec uses $\mathcal{L} + \lambda_{KD}\mathcal{L}_{KD}$ and \mathcal{L}_D to train the generator and discriminators alternately, where λ_{KD} is hyperparameter. Through training, the streamable APCodec aims to approach the decoded audio quality of the non-streamable APCodec while maintaining its advantage of low latency.

IV. EXPERIMENTS

A. Data and Feature Configuration

A subset of the VCTK-0.92 corpus [42] which contained approximately 43 hours of 48 kHz speech recordings from 108 speakers with various accents, was adopted in our experiments. We selected 40,936 utterances from 100 speakers as the training set. Then we built the test set, which included 2,937 utterances from remaining 8 unseen speakers. The original 48 kHz waveforms and downsampled waveforms at 24 kHz and 16 kHz were used for the experiments (i.e., $f_s = 48000$ or 24000 or 16000). When extracting the amplitude spectra, phase spectra and mel spectrograms from natural waveforms, the window size was 320 samples (i.e., $w_l = 320$), the window shift was 40 samples (i.e., $w_s = 40$), and the FFT point number was 1024 (i.e., $N = 513$). This configuration is applicable to waveforms at all sampling rates.

B. Model Details

In our experiments¹, we compared the proposed APCodec with four well-known neural waveform codecs, i.e., SoundStream [25], Encodec [26], HiFi-Codec [29] and AudioDec [33]. The descriptions of these codecs are as follows.

- **SoundStream**: The SoundStream [25] audio codec. We reimplemented it using the open source implementation². The downsampling/upsampling ratio was 320. It can achieve low-latency streamable inference.
- **Encodec**: The Encodec [26] audio codec. We reimplemented it using the open source implementation². The downsampling/upsampling ratio was also 320. It can also achieve low-latency streamable inference.
- **HiFi-Codec**: The HiFi-Codec [29] audio codec. We reimplemented it using the open source implementation². The downsampling/upsampling ratio was also 320. However, the HiFi-Codec is non-streamable, and there is no streamable implementation provided in the open-source code.
- **AudioDec**: The AudioDec [33] audio codec. It is specifically designed for 48 kHz audio codec. We reimplemented the *AudioDec v1* model in [33] which has been confirmed to deliver the best performance using the open source implementation³. This model integrates both the encoder and the HiFi-GAN vocoder. Therefore, the *AudioDec v1* model is not an end-to-end model. The downsampling/upsampling ratio for the model was 320. The AudioDec can also achieve low-latency streamable inference.
- **APCodec**: The proposed non-streamable APCodec. In the encoder and decoder, the kernel size for all convolutional operations was set to 7. The kernel size for two deconvolutional operations was set to 16. The channel size C , C_H and N_c were 256, 512 and 32, respectively. The downsampling/upsampling ratio was $D = 8$. Fig. 1 serves as an example of a 48 kHz audio codec, showcasing the sampling rates of the spectral characteristics and latent codes. We can observe that the APCodec only requires $8\times$ downsampling to encode a latent code with a sampling rate as low as 150 Hz. The hyperparameters for loss functions were set as $\lambda_P = \frac{20}{9}$, $\lambda_{RI} = 2.25$, $\lambda_S = \frac{4}{9}$, $\lambda_M = 1$, $\lambda_{spec} = 45$, $\lambda_Q = 7.5$, and $\lambda_{MRD} = 0.1$. The model was trained using the AdamW optimizer [43] with $\beta_1 = 0.8$ and $\beta_2 = 0.99$ on a single NVIDIA RTX 3090 GPU. The learning rate decay was scheduled by a 0.999 factor in every epoch with an initial learning rate of 0.0002. The batch size was 16, and the truncated waveform length was 7960 samples for each training step. The model was trained until 1M steps.
- **APCodec-S**: The proposed streamable APCodec. It was modified according to the methods outlined in Section III-C for the **APCodec**, wherein the number of nodes in the replaced feed-forward layers remain consistent with the original convolutional layers' channel size. The hyperparameter for knowledge distillation was set as $\lambda_{KD} = 1$. Other training strategies were consistent with those used in **APCodec**.

These codecs were comparable because they all employed the similar quantization method (i.e., RVQ or related strategy). All of the above codecs adopted 1024 vectors (i.e., $M = 1024$)

¹Source codes will be released after paper acceptance. Examples of generated speech can be found at <https://yangai520.github.io/APCodec>.

²<https://github.com/yangdongchao/AcademiCodec>.

³<https://github.com/facebookresearch/AudioDec>.

in the codebook of each VQ. We conducted experiments at all three sampling rates, with two bitrates (low and high) tested at each sampling rate. However, since the **AudioDec** was originally designed for 48 kHz audio codec, its experiments were conducted only at a sampling rate of 48 kHz. For 48 kHz audio codecs, the bitrates were set at 6 kbps and 12 kbps, respectively. For 24 kHz audio codecs, the bitrates were set at 3 kbps and 6 kbps, respectively. For 16 kHz audio codecs, the bitrates were set at 2 kbps and 4 kbps, respectively. The configuration of low bitrate and high bitrate for **SoundStream**, **Encodec**, **AudioDec**, **APCodec** and **APCodec-S** was achieved by setting the number of VQs within the quantizer to $Q = 4$ and $Q = 8$, respectively. Due to the adoption of the GRVQ quantization strategy in **HiFi-Codec**, it employed two groups of RVQ, each consisting of 2 and 4 VQs, for achieving encoding for both low and high bitrates, respectively.

C. Evaluation Metrics

We comprehensively evaluated the performance of these compared audio codecs using multiple metrics. These metrics were specifically designed to evaluate the amplitude spectrum quality, overall audio quality, intelligibility, phase spectrum quality, generation speed and model complexity, respectively.

- **Amplitude spectrum quality:** The commonly used log-spectral distance (LSD) and mel-cepstrum distortion (MCD) were employed to evaluate the amplitude spectrum quality between the decoded audio \hat{x} generated by a codec and the natural one x . The LSD and MCD respectively represented the distortion of audio in the log amplitude spectral domain and the mel cepstral domain. A smaller result indicates less distortion.
- **Intelligibility:** The commonly used short-time objective intelligibility (STOI) [44] was used to quantify the intelligibility of \hat{x} , with natural audio x as the reference. The STOI score ranges from 0 to 1. A higher STOI score indicates that the speech is more easily understandable to humans.
- **Overall audio quality:** The commonly used virtual speech quality objective listener (ViSQOL)⁴ [45] tool was used to assess the overall quality of the decoded audio \hat{x} , with natural audio x as the reference. The ViSQOL outputs a mean opinion score - listening quality objective (MOS-LQO) score, where a higher score indicates better audio quality. The ViSQOL supports only two sampling rates: 48 kHz and 16 kHz. For 48 kHz ViSQOL, the MOS-LQO ranges from 1 to 4.75. For 16 kHz ViSQOL, the MOS-LQO ranges from 1 to 5.
- **Phase spectrum quality:** One of the highlights of the proposed APCodec lies in the phase modeling. To validate the effectiveness of phase modeling, the anti-wrapping phase distance (AWPD) proposed in our previous work [46], was employed to evaluate the phase spectrum quality between \hat{x} and x . Similar to the mentioned phase loss in Section III-B1, the AWPD was also computed separately for instantaneous phase, group

delay, and instantaneous angular frequency (denoted as $AWPD_{IP}$, $AWPD_{GD}$ and $AWPD_{IAF}$, respectively). After the activation of phase errors using the anti-wrapping function f_{AW} , the APDW is calculated in a manner akin to LSD, allowing it to accurately depict the actual phase distortion. A smaller result indicates less distortion.

- **Generation speed:** The real-time factor (RTF), which is defined as the ratio between the time consumed to generate audio waveforms and the duration of the generated audio waveforms, was utilized to evaluate the generation speed of a codec. In our implementation, the RTF value was calculated as the ratio between the time consumed to generate all test sentences using a single NVIDIA RTX 3090 GPU or a single Intel Xeon E5-2680 CPU core and the total duration of the test set. A lower RTF indicates a faster generation speed.
- **Model complexity:** The model size (excluding the discriminators) is used to measure the complexity of the codec model. For the application of audio codecs on certain embedded devices, a lightweight model is crucial.

D. Primary Experimental Results

The primary experiments aim to compare the performance differences between our proposed APCodec and other neural codecs. The APCodec is designed for high sampling rates and low bitrates, thus we focus our analysis on the audio codec results at a 48 kHz sampling rate. The experimental results at 48 kHz are depicted in Table I and Table II. It can be observed that at a sampling rate of 48 kHz and a bitrate of 6 kbps (low bitrate), without considering latency, our proposed APCodec achieved state-of-the-art (SOTA) performance across various metrics. Surprisingly, the ViSQOL score of the APCodec reached 4.07.

Specifically, we first compared the **HiFi-Codec** and **AP-Codec** because both of them were non-streamable. As shown in Table I, at a sampling rate of 48 kHz and a bitrate of 6 kbps, the proposed APCodec outperformed the HiFi-Codec significantly for all metrics. From the perspective of LSD and MCD, the APCodec exhibited higher quality in decoded audio amplitude spectrum, highlighting its advantage in explicitly modeling amplitude spectra. Similarly, according to the results of the AWPD metrics, it is evident that explicit modeling of phase spectra in the APCodec contributed to improving the precision of decoded phases. However, among the three specific metrics of AWPD, the difference reflected by $AWPD_{IP}$ was more pronounced. Although the APCodec outperformed the HiFi-Codec in both $AWPD_{GD}$ and $AWPD_{IAF}$ metrics, the numerical difference was very small. Overall, the $AWPD_{GD}$ values for all the codecs were concentrated in the range of 1.40 to 1.44, while the $AWPD_{IAF}$ values were concentrated in the range of 1.44 to 1.47. Additionally, we also observed that, apart from the proposed APCodec and APCodec-S, the $AWPD_{IP}$ values for other baseline codecs were all around 1.80. The shared characteristic among these codecs is the absence of explicit phase modeling. Consequently, we hypothesize that their $AWPD_{IP}$ values may reflect a consistent initial phase error. The APCodec we proposed achieved a reduction of

⁴<https://github.com/google/viqol>.

TABLE I

EXPERIMENTAL RESULTS OF AMPLITUDE SPECTRUM QUALITY, INTELLIGIBILITY, OVERALL AUDIO QUALITY AND PHASE SPECTRUM QUALITY FOR COMPARED CODECS ON THE TEST SET OF THE VCTK DATASET AT THREE SAMPLING RATES AND TWO BITRATES. THE **BOLD** AND UNDERLINE NUMBERS INDICATE THE OPTIMAL AND SUB-OPTIMAL RESULTS, RESPECTIVELY.

Codec	Low-latency (Streamable)	Sampling rate	Bitrate	LSD (dB)↓	MCD (dB)↓	STOI↑	ViSQOL↑	AWPD _{IP} (rad)↓	AWPD _{GD} (s)↓	AWPD _{IAF} (rad/s)↓
SoundStream	Yes	48 kHz	6 kbps	0.937	2.80	0.794	3.11	1.80	1.43	<u>1.45</u>
Encodect	Yes			1.04	2.61	0.793	3.31	1.80	1.43	1.47
HiFi-Codec	No			0.913	2.44	0.852	3.33	1.80	1.42	<u>1.45</u>
AudioDec	Yes			0.847	2.85	0.804	<u>3.98</u>	1.81	1.44	1.46
APCodec	No			0.818	1.60	0.875	4.07	1.68	1.40	1.44
APCodec-S	Yes			<u>0.835</u>	<u>1.67</u>	<u>0.865</u>	3.93	<u>1.74</u>	<u>1.41</u>	<u>1.45</u>
SoundStream	Yes	48 kHz	12 kbps	0.917	2.50	0.831	3.32	1.79	1.43	1.45
Encodect	Yes			0.885	2.17	0.860	3.51	1.79	1.42	1.45
HiFi-Codec	No			0.829	1.49	0.941	3.88	1.79	<u>1.40</u>	<u>1.44</u>
AudioDec	Yes			0.831	2.31	0.825	<u>4.14</u>	1.81	1.44	1.46
APCodec	No			0.796	1.33	0.901	4.26	1.60	1.38	1.42
APCodec-S	Yes			<u>0.822</u>	<u>1.42</u>	<u>0.903</u>	4.13	<u>1.70</u>	<u>1.40</u>	<u>1.44</u>
SoundStream	Yes	24 kHz	3 kbps	0.977	3.03	0.804	–	<u>1.79</u>	1.40	<u>1.44</u>
Encodect	Yes			0.958	2.74	0.817	–	<u>1.79</u>	1.39	<u>1.44</u>
HiFi-Codec	No			<u>0.849</u>	2.10	0.875	–	<u>1.79</u>	1.36	<u>1.44</u>
APCodec	No			0.839	<u>2.31</u>	<u>0.856</u>	–	1.66	1.36	1.42
SoundStream	Yes	24 kHz	6 kbps	0.944	2.7	0.832	–	1.78	1.38	1.44
Encodect	Yes			0.933	2.53	0.836	–	1.78	1.38	1.44
HiFi-Codec	No			0.850	1.83	0.910	–	<u>1.77</u>	<u>1.35</u>	<u>1.43</u>
APCodec	No			0.815	<u>2.02</u>	<u>0.877</u>	–	1.60	1.34	1.41
SoundStream	Yes	16 kHz	2 kbps	0.965	3.11	0.804	3.62	<u>1.78</u>	1.36	1.44
Encodect	Yes			0.939	2.98	0.810	3.70	<u>1.78</u>	1.36	<u>1.43</u>
HiFi-Codec	No			0.910	2.49	0.832	3.84	1.79	<u>1.35</u>	<u>1.43</u>
APCodec	No			0.834	2.48	0.852	4.09	1.68	1.33	1.41
SoundStream	Yes	16 kHz	4 kbps	0.938	2.76	0.837	3.83	<u>1.76</u>	1.35	1.43
Encodect	Yes			0.928	2.78	0.823	3.77	1.77	1.35	1.43
HiFi-Codec	No			0.875	2.14	0.869	4.10	1.77	<u>1.33</u>	<u>1.42</u>
APCodec	No			0.792	2.12	0.885	4.32	1.56	1.29	1.38

approximately 0.12 in the $AWPD_{IP}$ value through explicit prediction and optimization of the phase. The aforementioned findings suggested a similarity in the phase spectrum continuity of the decoded audio across these codecs according to the results of $AWPD_{GD}$ and $AWPD_{IAF}$. Nevertheless, the **APCodec** stood out by producing audio with instantaneous phase values that closely aligned with the natural phase, showcasing superior quality in decoded phase. The aforementioned advantages also contributed to **APCodec**'s leading position in intelligibility (i.e., STOI) and overall audio quality (i.e., ViSQOL). In terms of generation efficiency, as shown in Table II, whether on GPU or CPU, the **APCodec** exhibited faster generation speed than the **HiFi-Codec**. This advantage was more pronounced when running on CPU. This phenomenon indicated that without the parallel acceleration of GPU, utilizing spectra as encoding and decoding objects can significantly enhance generation efficiency compared to the direct encoding and decoding of waveforms. Especially for high-sampling-rate audio codecs, the spectrum-based approach was more suitable due to the larger number of waveform samples. Furthermore, the **APCodec** was a lightweight model, with a model size of only 26.9% compared to that of the **HiFi-Codec**. Therefore, despite the HiFi-Codec [29] incorporating GRVQ to reduce bitrates, its performance in low bitrate scenarios was not as effective as our proposed **APCodec**.

Then, we compared the **APCodec-S** with other streamable codecs, i.e., **SoundStream**, **Encodect** and **AudioDec** at 48 kHz and 6 kbps. To ensure the generation of at least one frame of latent code, the minimum length of the input audio for these codecs is 320 samples. Therefore, the latency for these codecs is approximately 6.67 ms for 48 kHz audio. As shown in Table I, the proposed **APCodec-S** significantly outperformed the baseline **SoundStream** and **Encodect** on all metrics. However, we found that the **AudioDec**, which is a combination of encoder and vocoder, served as a robust baseline, with a ViSQOL score 0.05 higher than the **APCodec-S**. Yet, it lagged behind the **APCodec-S** in all other metrics. As illustrated in Table II, the generation speed of the **SoundStream** and **Encodect** was relatively fast, slightly trailing behind the **APCodec-S**, but their model size was 1.78 times that of the **APCodec-S**. The generation speed of the **AudioDec** on CPU was relatively slow, just reaching the real-time standard. This may be attributed to the introduction of the HiFi-GAN vocoder. The introduction of the vocoder also resulted in a large model size, approximately 6.4 times that of the **APCodec-S**. Furthermore, the two-stage training paradigm of the **AudioDec** also led to operational complexity, in contrast to our proposed end-to-end **APCodec**.

By comparing the **APCodec** and **APCodec-S** at 48 kHz and 6 kbps in Table I, the overall performance of the streamable model decreased compared to non-streamable one. This is reasonable, as the streamable model did not leverage future

TABLE II

EXPERIMENTAL RESULTS OF GENERATION SPEED AND MODEL COMPLEXITY FOR COMPARED CODECS ON THE TEST SET OF THE VCTK DATASET AT 48 KHZ SAMPLING RATE AND TWO BITRATES. HERE, “ $a\times$ ” REPRESENTS $a\times$ REAL TIME. THE **BOLD** AND UNDERLINE NUMBERS INDICATE THE OPTIMAL AND SUB-OPTIMAL RESULTS, RESPECTIVELY.

Codec	Bitrate	RTF (GPU) \downarrow	RTF (CPU) \downarrow	Model size \downarrow
SoundStream	6 kbps	0.0148 (67.6 \times)	0.231 (4.33 \times)	83.2M
Encodec		0.0149 (67.1 \times)	0.232 (4.31 \times)	83.2M
HiFi-Codec		0.0178 (56.2 \times)	0.878 (1.14 \times)	243M
AudioDec		0.0135 (74.1 \times)	0.771 (1.30 \times)	108M
APCodec		0.0112 (89.3 \times)	0.173 (5.78 \times)	<u>65.4M</u>
APCodec-S		0.0109 (91.7\times)	0.112 (8.93\times)	46.8M
SoundStream	12 kbps	0.0160 (62.5 \times)	0.236 (4.24 \times)	99.2M
Encodec		0.0157 (63.7 \times)	0.238 (4.20 \times)	99.2M
HiFi-Codec		0.0178 (56.2 \times)	0.921 (1.09 \times)	243M
AudioDec		0.0132 (75.8 \times)	0.780 (1.28 \times)	110M
APCodec		0.0120 (83.3 \times)	0.181 (5.52 \times)	<u>66.0M</u>
APCodec-S		0.0119 (84.0\times)	0.116 (8.62\times)	47.4M

information. The **APCodec** can be considered as an upper-bound model for the **APCodec-S**. Nevertheless, the **APCodec-S** still outperformed numerous streamable baselines. It’s worth mentioning that the **APCodec-S** had an increase of 0.06 in $AWPD_{IP}$ metric compared to the **APCodec**. Although this difference was small, during the training process, we clearly observed that the AW-IP loss reduction was challenging for the **APCodec-S**. This also reflects that in our proposed model, the convergence status of the AW-IP loss can be used to preliminarily estimate the quality of the decoded audio, which is helpful for model selection. Finally, compared to the **APCodec**, the **APCodec-S** showed improved efficiency and a further reduction in model size, as shown in Table II. This is because, in the process of transforming the non-streamable model into a streamable one, we chose to replace non-causal convolutions with feed-forward layers instead of causal convolutions used in SoundStream, Encodec and AudioDec. This reduced the model complexity and further improved the generation speed.

To further assess the performance of the codecs at different bitrates, we conducted experiments on these comparative codecs at 48 kHz and 12 kbps. The results are also presented in Tables I and II. For the same codec, there was a noticeable improvement in aspects such as amplitude spectrum quality, intelligibility, overall audio quality and phase spectrum quality at 12 kbps compared to those at 6 kbps. Simultaneously, the former experienced a decrease in generation speed, coupled with an increase in model complexity. This is reasonable, as increasing the number of VQs can reduce the quantization error and increase trainable parameters. The comparison results for different codecs at 12 kbps were essentially consistent with those at 6 kbps. Notably, the ViSQOL score for the **APCodec** at 12 kbps reached an impressive 4.26 (the maximum score is 4.75). Slightly differently, the performance of the **HiFi-Codec** at 12 kbps was significantly stronger than that at 6 kbps. Specifically, at 12 kbps, the **HiFi-Codec** even achieved the highest intelligibility, according to the results of STOI. In addition, the **AudioDec** also demonstrated a noticeable performance improvement at 12 kbps. This result aligns with expectations, as the AudioDec [33] was originally designed as a 48 kHz audio codec for 12.8 kbps. This observation

underscored the suitability of the proposed **APCodec** for encoding and decoding at low bitrates, showcasing enhanced audio compression capabilities.

Due to their original design as low sampling rate (e.g., 16 kHz or 24 kHz) audio codecs of the SoundStream, Encodec and HiFi-Codec, we also conducted comparative experiments at sampling rates of 16 kHz and 24 kHz. For simplicity, the streamable **APCodec** was not included in the experiments, and the AudioDec was also excluded due to its original design for 48 kHz. The experimental results are shown in Table I, where the ViSQOL at 24 kHz is not calculated as it is not supported at that sampling rate. It can be observed that both the **SoundStream** and **Encodec** still exhibited significant gaps compared to the **APCodec** at these two sampling rates. At 16 kHz, the **APCodec** surpassed the **HiFi-Codec** across all metrics. However, at 24 kHz, the **APCodec** did not perform as well as the **HiFi-Codec** in terms of MCD and STOI. Furthermore, it can be noted that in some other metrics (e.g., ViSQOL score), the difference between the **HiFi-Codec** and **APCodec** was not as pronounced as it was at 48 kHz. This may be attributed to the fact that the HiFi-Codec is originally designed for 16 kHz and 24 kHz codecs. The above results indicated that while our proposed **APCodec** exhibited a more pronounced advantage at 48 kHz, applying it at lower sampling rates also yielded good performance.

Based on the above experimental results, we can conclude that **APCodec**, by leveraging the advantages of parametric codec and waveform codec, is better suited for audio encoding and decoding at both high sampling rates and low bitrates. The **APCodec** possesses the advantages of high decoded audio quality, low compression rate, fast generation speed, low model complexity, and low latency.

E. Analysis and Discussion

We conducted additional analytical experiments, discussing the roles of the proposed structures and losses in **APCodec** through ablation studies. Simultaneously, we explored the performance of **APCodec** on various other types of audio. For simplicity, the experiments were conducted only at sampling rate of 48 kHz and bitrate of 6 kbps.

1) *Ablation Studies*: We conducted six ablation experiments to validate the roles of certain structures and losses in the **APCodec**. The effects of other structures and losses have been confirmed in our previous publication [38]. For the **APCodec**, the descriptions of the ablation variants for comparison are as follows.

- **APCodec w/o CNV**: Ablating the modified ConvNeXt v2 network and replacing it with the residual convolutional network (RCNet) as utilized in [28], [37], [38].
- **APCodec w/o MelMSE**: Ablating the MSE loss on mel spectrograms from \mathcal{L}_M in Equation 16.
- **APCodec w/o QLoss**: Ablating the quantization loss \mathcal{L}_Q in Equation 18.
- **APCodec w/o MRD**: Ablating the MRD in the GAN-based loss and replacing it with the multi-scale discriminator (MSD) as utilized in [28], [38].

TABLE III

EXPERIMENTAL RESULTS OF AMPLITUDE SPECTRUM QUALITY, INTELLIGIBILITY, OVERALL AUDIO QUALITY AND PHASE SPECTRUM QUALITY FOR ABLATED CODECS ON THE TEST SETS OF THE VCTK DATASET FOR SAMPLING RATE OF 48 KHZ AND BITRATE OF 6 KBPS. THE **BOLD** NUMBERS INDICATE THE OPTIMAL RESULTS.

Codec	LSD (dB)↓	STOI↑	ViSQOL↑	AWPD _{IP} (rad)↓
APCodec	0.818	0.875	4.07	1.68
APCodec w/o CNV	0.889	0.813	3.57	1.81
APCodec w/o MelMSE	0.830	0.830	3.79	1.65
APCodec w/o QLoss	0.841	0.841	3.74	1.70
APCodec w/o MRD	0.825	0.874	3.95	1.70
APCodec w/o Hinge	0.823	0.879	3.92	1.67
APCodec-S	0.835	0.865	3.93	1.74
APCodec-S w/o KD	0.842	0.864	3.92	1.79

- **APCodec w/o Hinge**: Ablating the adversarial loss in the form of hinge GAN and adopting the one in the form of least squares GAN as utilized in [28], [38].

For the **APCodec-S**, the description of the ablation variant for comparison is as follows.

- **APCodec-S w/o KD**: Ablating the knowledge distillation loss \mathcal{L}_{KD} , i.e., training the streamable student model directly without the guidance of the teacher model.

The results of the ablation experiments are shown in Table III. For simplicity, only the LSD, STOI, ViSQOL and AWPD_{IP} metrics were used. By comparing the **APCodec** and **APCodec w/o CNV**, it can be observed that replacing the modified ConvNeXt v2 network with RCNet resulted in a significant decrease in all metrics. Specifically, the **APCodec w/o CNV**'s ViSQOL score decreased by 0.5 compared to the **APCodec**, indicating a significant distortion in the overall audio quality. Additionally, it's worth noting that the **APCodec w/o CNV**'s AWPD_{IP} metric became as poor as the **SoundStream**, **Encodec**, **HiFi-Codec** and **AudioDec**. This indicates that the RCNet impeded the learning of phase information, contradicting the conclusions in [37] and [38]. Hence, the RCNet was apt for tasks involving phase predictions [37] and vocoders [28], [38], leveraging its cumulative dilated convolutional layers to broaden the receptive field. Nevertheless, in codec tasks that necessitated a more sophisticated phase modeling, the RCNet exhibited an inadequate modeling capability. The ConvNeXt v2 network, borrowed from the field of image processing, exhibited stronger modeling capabilities, making it well-suited for the design of codec models.

Regarding the ablation studies on some training strategies, by comparing the **APCodec** and **APCodec w/o MelMSE**, it is evident that the MSE loss on the mel spectrogram had a positive impact on intelligibility and overall audio quality. The MSE exhibited greater sensitivity to outliers when compared to MAE. It can be viewed as a complement to MAE, collectively enhancing the overall quality of the mel spectrogram. Derived from the outcomes of the LSD and AWPD_{IP}, it is evident that the influence of this MSE loss on amplitude and phase learning was contradictory. Enhancing the quality of the amplitude spectrum unavoidably came at the expense of compromising the quality of the phase spectrum. By comparing the **APCodec** and **APCodec w/o QLoss**, it can

TABLE IV

EXPERIMENTAL RESULTS OF AMPLITUDE SPECTRUM QUALITY, OVERALL AUDIO QUALITY AND PHASE SPECTRUM QUALITY FOR THE COMPARISON BETWEEN **HiFi-CODEC** AND **APCODEC** AND THE COMPARISON BETWEEN **AUDIODEC** AND **APCODEC-S** ON THE TEST SETS OF THE OPENCPOP DATASET AND FSD50K DATASET FOR SAMPLING RATE OF 48 KHZ AND BITRATE OF 6 KBPS. THE **BOLD** NUMBERS INDICATE THE OPTIMAL RESULTS.

Dataset	Codec	LSD (dB)↓	ViSQOL↑	AWPD _{IP} (rad)↓
Opencpop	HiFi-Codec	1.08	3.52	1.80
	APCodec	0.864	4.21	1.67
	AudioDec	0.967	4.10	1.81
	APCodec-S	0.964	4.06	1.74
FSD50K	HiFi-Codec	1.17	3.18	1.81
	APCodec	0.845	3.93	1.71
	AudioDec	1.01	3.75	1.82
	APCodec-S	0.874	3.84	1.76

be observed that the quantization loss had a significant impact on the amplitude spectrum quality, intelligibility, and overall audio quality, while its influence on the phase spectrum quality was relatively minor. The incorporation of quantization loss effectively alleviated quantization errors, thereby contributing to the enhancement of APCodec's performance. Replacing MRD with MSD significantly impacted the amplitude spectrum quality and overall audio quality, based on the results of the **APCodec w/o MRD**. This is in line with expectations because the MRD focused more on the quality of the amplitude spectrum, making it suitable for our spectrum-based approach. Finally, the hinge-form adversarial loss was more effective compared to the least-squares-form adversarial loss commonly used in some vocoder tasks [28], [38], according to the results of the **APCodec w/o Hinge**. In terms of auditory sensation, the **APCodec w/o Hinge** experienced very apparent harsh noise.

In terms of the role of the proposed knowledge distillation strategy for the streamable APCodec, we compared the **APCodec-S** and **APCodec-S w/o KD**. The results are also listed in Table III. It can be observed that without the guidance of the non-streamable teacher model, the streamable student model exhibited slight decreases across all metrics. In particular, the AWPD_{IP} of the **APCodec-S w/o KD** deteriorated to the level of the initial phase error, resembling the patterns seen in **SoundStream**, **Encodec**, **HiFi-Codec** and **AudioDec**. This indicates that the low-latency implementation on model structures discussed in Section III-C hindered the learning of phase, and accurate phase prediction required a network with a broader receptive field. The knowledge distillation strategy can effectively alleviate the challenge of phase learning difficulty (AWPD_{IP} reduced by 0.05), thereby promoting overall audio quality improvement.

2) *Validation on Diverse Audio Datasets*: Since the VCTK is a speech dataset, to assess the performance of the proposed APCodec on different types of audio datasets, we incorporated two additional datasets. These two additional datasets included: Opencpop [47], a publicly available high quality Mandarin singing corpus of approximately 5.2 hours designed for singing voice synthesis; FSD50K [48], an open dataset of approximately 391 hours for human-labeled sound

events. For the Opencpop dataset, we utilized the officially pre-trimmed data, selecting 3,367 utterances as the training set and the remaining 389 utterances as the test set. For the FSD50K dataset, 40,966 utterance and 10,231 utterances were respectively chosen as the training set and test set. The sampling rates for the Opencpop and FSD50K datasets are both 44.1 kHz. We upsampled them to 48 kHz for experiments.

For the sake of fairness and simplicity, we compared the performance between non-streamable **HiFi-Codec** and **APCodec**, as well as the performance between streamable **AudioDec** and **APCodec-S**, respectively. These models were further finetuned for 200k steps each on the Opencpop and FSD50K datasets, based on the well-trained models using the VCTK dataset. We separately calculated the objective metrics for the Opencpop and FSD50K datasets on their respective test sets, and the results are shown in Table IV. Due to the fact that the STOI is typically used solely for assessing speech intelligibility, we exclusively employed the LSD, ViSQOL, and AWPDI_P metrics in this experiment. It can be observed that, whether on the Opencpop or the FSD50K dataset, the performance for all metrics of the **APCodec** was significantly better than that of the **HiFi-Codec**. Specifically, on the sound event dataset (i.e., FSD50K), the performance of the **HiFi-Codec** noticeably declined compared to its performances on datasets like VCTK and Opencpop, which involve human vocalizations. However, our proposed **APCodec** still managed to maintain good performance. In comparison between the **AudioDec** and **APCodec-S** on the Opencpop dataset, the gap between the LSD of the **AudioDec** and the LSD of the **APCodec-S** significantly narrowed, compared to the results on the VCTK dataset. The **AudioDec** even led by 0.04 on the ViSQOL score. However, on the FSD50K dataset, all metrics of the **AudioDec** were inferior to those of the **APCodec-S**. The above experimental results fully demonstrated that our proposed **APCodec** exhibited strong generalization and adaptability on other types of datasets, especially on non-human vocalization datasets, compared to other mainstream neural codecs. Thus, the **APCodec** is more suitable for various audio signal processing tasks which will also be a focus of our future work.

V. CONCLUSION

In this paper, we proposed a novel neural audio codec called **APCodec**. The **APCodec** leveraged the advantages of parametric codecs, regarding the audio amplitude and phase spectra as parametric characteristics rather than the raw waveforms for parallel encoding and parallel decoding. Thus, it could obtain latent codes at low sampling rate using very minimal downsampling operations. To ensure the fidelity of the decoded audio similar to waveform codecs, spectral-level loss, quantization loss, and GAN-based loss were employed to train the **APCodec** model. We also constructed a low-latency streamable **APCodec** by combining feed-forward layers and causal convolution layers with knowledge distillation training strategies. Experimental results confirm that our proposed **APCodec** exhibited advantages at high waveform sampling rates and low bitrates, demonstrating high-quality decoded audio,

low compression rate, fast generation speed, low model complexity, and low latency. It surpassed the performance of the baseline **SoundStream**, **Encodec**, **HiFi-Codec** and **AudioDec**. Further analysis experiments also confirmed the effectiveness of the structure and loss proposed in **APCodec**, as well as its versatility and generalizability across diverse audio datasets.

In future work, we will 1) attempt to use features from other spectral domains, such as MDCT spectrum, as encoding and decoding objects to further enhance the training and generation efficiency of the existing framework of **APCodec**; 2) apply the **APCodec** to downstream tasks such as TTS and speech enhancement (SE), aiming to create more advanced results.

REFERENCES

- [1] K. Brandenburg and G. Stoll, "ISO/MPEG-1 audio: A generic standard for coding of high-quality digital audio," *Journal of the Audio Engineering Society*, vol. 42, no. 10, pp. 780–792, 1994.
- [2] T. Treiman, "Linear predictive coding systems," in *Proc. ICASSP*, vol. 1, 1976, pp. 474–478.
- [3] P. Kroon, E. Deprettere, and R. Sluyter, "Regular-pulse excitation—a novel approach to effective and efficient multipulse coding of speech," *IEEE transactions on acoustics, speech, and signal processing*, vol. 34, no. 5, pp. 1054–1063, 1986.
- [4] R. Salami, C. Laffamme, J.-P. Adoul, and D. Massaloux, "A toll quality 8 kb/s speech codec for the personal communications system (pcs)," *IEEE Transactions on Vehicular Technology*, vol. 43, no. 3, pp. 808–816, 1994.
- [5] Z. Borsos, R. Marinier, D. Vincent, E. Kharitonov, O. Pietquin, M. Sharifi, D. Roblek, O. Teboul, D. Grangier, M. Tagliasacchi *et al.*, "AudioLM: A language modeling approach to audio generation," *IEEE/ACM Transactions on Audio, Speech, and Language Processing*, vol. 31, pp. 2523–2533, 2023.
- [6] C. Wang, S. Chen, Y. Wu, Z. Zhang, L. Zhou, S. Liu, Z. Chen, Y. Liu, H. Wang, J. Li *et al.*, "Neural codec language models are zero-shot text to speech synthesizers," *arXiv preprint arXiv:2301.02111*, 2023.
- [7] X. Zhang, D. Zhang, S. Li, Y. Zhou, and X. Qiu, "SpeechTokenizer: Unified speech tokenizer for speech large language models," *arXiv preprint arXiv:2308.16692*, 2023.
- [8] Z. Huang, C. Meng, and T. Ko, "RepCodec: A speech representation codec for speech tokenization," *arXiv preprint arXiv:2309.00169*, 2023.
- [9] Y. Ren, T. Wang, J. Yi, L. Xu, J. Tao, C. Zhang, and J. Zhou, "Fewer-token neural speech codec with time-invariant codes," *arXiv preprint arXiv:2310.00014*, 2023.
- [10] D. O'Shaughnessy, "Linear predictive coding," *IEEE potentials*, vol. 7, no. 1, pp. 29–32, 1988.
- [11] J.-M. Valin, G. Maxwell, T. B. Terriberry, and K. Vos, "High-quality, low-delay music coding in the opus codec," in *Audio Engineering Society Convention 135*, 2013.
- [12] M. Dietz, M. Multrus, V. Eksler, V. Malenovsky, E. Norvell, H. Pobloth, L. Miao, Z. Wang, L. Laaksonen, A. Vasilache *et al.*, "Overview of the EVS codec architecture," in *Proc. ICASSP*, 2015, pp. 5698–5702.
- [13] W. B. Kleijn, F. S. Lim, A. Luebs, J. Skoglund, F. Stimberg, Q. Wang, and T. C. Walters, "WaveNet based low rate speech coding," in *Proc. ICASSP*, 2018, pp. 676–680.
- [14] J. Klejsa, P. Hedelin, C. Zhou, R. Fejgin, and L. Villemoes, "High-quality speech coding with sample RNN," in *Proc. ICASSP*, 2019, pp. 7155–7159.
- [15] J.-M. Valin and J. Skoglund, "A real-time wideband neural vocoder at 1.6 kb/s using LPCNet," in *Proc. Interspeech*, 2019, pp. 3406–3410.
- [16] A. Mustafa, J. Bütthe, S. Korse, K. Gupta, G. Fuchs, and N. Pia, "A streamwise GAN vocoder for wideband speech coding at very low bit rate," in *Proc. WASPAA*, 2021, pp. 66–70.
- [17] Y. Zheng, L. Xiao, W. Tu, Y. Yang, and X. Xu, "CQNV: A combination of coarsely quantized bitstream and neural vocoder for low rate speech coding," *arXiv preprint arXiv:2307.13295*, 2023.
- [18] G. Davidson, M. Vinton, P. Ekstrand, C. Zhou, L. Villemoes, and L. Lu, "High quality audio coding with MDCTNet," in *Proc. ICASSP*, 2023, pp. 1–5.
- [19] H. Lim, J. Lee, B. H. Kim, I. Jang, and H.-G. Kang, "End-to-end neural audio coding in the MDCT domain," in *Proc. ICASSP*, 2023, pp. 1–5.

- [20] H. S. Black and J. Edson, "Pulse code modulation," *Transactions of the American Institute of Electrical Engineers*, vol. 66, no. 1, pp. 895–899, 1947.
- [21] S. Kankanahalli, "End-to-end optimized speech coding with deep neural networks," in *Proc. ICASSP*, 2018, pp. 2521–2525.
- [22] A. Van Den Oord, O. Vinyals *et al.*, "Neural discrete representation learning," in *Proc. NIPS*, vol. 30, 2017.
- [23] C. Gărbacea, A. van den Oord, Y. Li, F. S. Lim, A. Luebs, O. Vinyals, and T. C. Walters, "Low bit-rate speech coding with VQ-VAE and a WaveNet decoder," in *Proc. ICASSP*, 2019, pp. 735–739.
- [24] K. Zhen, J. Sung, M. S. Lee, S. Beack, and M. Kim, "Cascaded cross-module residual learning towards lightweight end-to-end speech coding," 2019, pp. 3396–3400.
- [25] N. Zeghidour, A. Luebs, A. Omran, J. Skoglund, and M. Tagliasacchi, "SoundStream: An end-to-end neural audio codec," *IEEE/ACM Transactions on Audio, Speech, and Language Processing*, vol. 30, pp. 495–507, 2021.
- [26] A. Défossez, J. Copet, G. Synnaeve, and Y. Adi, "High fidelity neural audio compression," *arXiv preprint arXiv:2210.13438*, 2022.
- [27] A. Vasuki and P. Vanathi, "A review of vector quantization techniques," *IEEE Potentials*, vol. 25, no. 4, pp. 39–47, 2006.
- [28] J. Kong, J. Kim, and J. Bae, "HiFi-GAN: Generative adversarial networks for efficient and high fidelity speech synthesis," in *Proc. NIPS*, vol. 33, 2020, pp. 17 022–17 033.
- [29] D. Yang, S. Liu, R. Huang, J. Tian, C. Weng, and Y. Zou, "HiFi-Codec: Group-residual vector quantization for high fidelity audio codec," *arXiv preprint arXiv:2305.02765*, 2023.
- [30] L. Xu, J. Jiang, D. Zhang, X. Xia, L. Chen, Y. Xiao, P. Ding, S. Song, S. Yin, and F. Sohel, "An intra-BRNN and GB-RVQ based end-to-end neural audio codec," in *Proc. Interspeech*, 2023, pp. 800–803.
- [31] T. Jenrungrot, M. Chinen, W. B. Kleijn, J. Skoglund, Z. Borsos, N. Zeghidour, and M. Tagliasacchi, "LMCodec: A low bitrate speech codec with causal transformer models," in *Proc. ICASSP*, 2023, pp. 1–5.
- [32] W. Xiao, W. Liu, M. Wang, S. Yang, Y. Shi, Y. Kang, D. Su, S. Shang, and D. Yu, "Multi-mode neural speech coding based on deep generative networks," in *Proc. Interspeech*, 2023, pp. 819–823.
- [33] Y.-C. Wu, I. D. Gebreu, D. Marković, and A. Richard, "AudioDec: An open-source streaming high-fidelity neural audio codec," in *Proc. ICASSP*, 2023, pp. 1–5.
- [34] J. L. Ba, J. R. Kiros, and G. E. Hinton, "Layer normalization," *arXiv preprint arXiv:1607.06450*, 2016.
- [35] S. Woo, S. Debnath, R. Hu, X. Chen, Z. Liu, I. S. Kweon, and S. Xie, "ConvNeXt v2: Co-designing and scaling convnets with masked autoencoders," in *Proc. CVPR*, 2023, pp. 16 133–16 142.
- [36] D. Hendrycks and K. Gimpel, "Gaussian error linear units (gelus)," *arXiv preprint arXiv:1606.08415*, 2016.
- [37] Y. Ai and Z.-H. Ling, "Neural speech phase prediction based on parallel estimation architecture and anti-wrapping losses," in *Proc. ICASSP*, 2023, pp. 1–5.
- [38] Y. Ai and Z.-H. Ling, "APNet: An all-frame-level neural vocoder incorporating direct prediction of amplitude and phase spectra," *IEEE/ACM Transactions on Audio, Speech, and Language Processing*, vol. 31, pp. 2145–2157, 2023.
- [39] W. Jang, D. Lim, J. Yoon, B. Kim, and J. Kim, "Univnet: A neural vocoder with multi-resolution spectrogram discriminators for high-fidelity waveform generation," *arXiv preprint arXiv:2106.07889*, 2021.
- [40] A. L. Maas, A. Y. Hannun, and A. Y. Ng, "Rectifier nonlinearities improve neural network acoustic models," in *Proc. ICML*, vol. 30, no. 1, 2013, p. 3.
- [41] K. Kumar, R. Kumar, T. de Boissiere, L. Gestin, W. Z. Teoh, J. Sotelo, A. de Brébisson, Y. Bengio, and A. C. Courville, "MelGAN: Generative adversarial networks for conditional waveform synthesis," *Advances in neural information processing systems*, vol. 32, 2019.
- [42] J. Yamagishi, C. Veaux, K. MacDonald *et al.*, "CSTR VCTK corpus: English multi-speaker corpus for CSTR voice cloning toolkit (version 0.92)," *University of Edinburgh. The Centre for Speech Technology Research (CSTR)*, 2019.
- [43] I. Loshchilov and F. Hutter, "Decoupled weight decay regularization," in *Proc. ICLR*, 2018.
- [44] C. H. Taal, R. C. Hendriks, R. Heusdens, and J. Jensen, "A short-time objective intelligibility measure for time-frequency weighted noisy speech," in *Proc. ICASSP*, 2010, pp. 4214–4217.
- [45] M. Chinen, F. S. Lim, J. Skoglund, N. Gureev, F. O’Gorman, and A. Hines, "ViSQOL v3: An open source production ready objective speech and audio metric," in *Proc. QoMEX*, 2020, pp. 1–6.
- [46] Y.-X. Lu, Y. Ai, H.-P. Du, and Z.-H. Ling, "Towards high-quality and efficient speech bandwidth extension with parallel amplitude and phase prediction," *arXiv preprint arXiv:2401.06387*, 2024.
- [47] Y. Wang, X. Wang, P. Zhu, J. Wu, H. Li, H. Xue, Y. Zhang, L. Xie, and M. Bi, "Openpop: A high-quality open source chinese popular song corpus for singing voice synthesis," *arXiv preprint arXiv:2201.07429*, 2022.
- [48] E. Fonseca, X. Favory, J. Pons, F. Font, and X. Serra, "FSD50K: An open dataset of human-labeled sound events," *IEEE/ACM Transactions on Audio, Speech, and Language Processing*, vol. 30, pp. 829–852, 2021.